Mechanics of Growth and Coalescence of Preexisting Voids

T. Jodlowski[1], J. Giovanola[1†]
[1] Ecole Polytechnique Fédérale, Lausanne, Switzerland;

This paper experimentally investigates the growth and coalescence of preexisting voids in a ductile matrix and presents quantitative kinetics data for these processes.

Leaded copper alloys have been selected as model materials, in which lead inclusions act as pre-existing voids – as demonstrated by unit cell numerical simulations for a wide range of stress states – and the varying alloy content of the ductile matrix results in different deformation and failure behaviors of the intervoid ligaments. The model materials are deformed and fractured in combined torsion / tension / compression tests and notched tensile tests to subject them to the desired wide range of stress triaxialities. Quantitative fractography and metallography provide the desired void kinetics data that can be correlated with numerical simulations and existing void growth and coalescence models.

The influence of stress-state and microstructural characteristics on void growth and on void coalescence will be illustrated at the hand of the preliminary results of the investigation.

1. Introduction

The long term goal of this research is to elucidate and model the mechanisms of ductile fracture in metals by void growth and coalescence under general loading conditions, i.e. low as well as high stress triaxialities. The specific objective of the current project is to quantify the growth of easily nucleated or preexisting voids and to establish the mechanisms of their coalescence to final fracture. The general research approach followed in the investigation is to combine non-standard experimental techniques with careful metallographic and fractographic observations, numerical simulations (single microscopic cell and complete specimens) and analytical modeling of the observed micromechanisms of fracture. We apply this approach to appropriately selected model materials that allow us to study independently various stages of the growth and coalescence mechanisms. This paper discusses techniques we developed in conjunction with a leaded brass as model material to observe and quantify ductile void growth kinetics under different stress states. We present our preliminary results for the model material tested (to very large strains) in pure torsion and tension-torsion and comment on the potential significance of these results.

† To whom all correspondence should be addressed.

2. Concept of model material and selection

Under model material, we understand a material, in which a specific ductile fracture mechanism is emphasized and easily observable and quantifiable. In the present study, we focus on void growth and coalescence, and we select several leaded copper alloys as model materials. These alloys offer the advantage of deforming to very large strains before failure and because voids form at the location of lead inclusions, their growth can easily be tracked and quantified. Further, if we assume that a very soft lead inclusion acts as a pre-existing void, the chosen model material allows us to decouple the void growth processes from void nucleation effects. To validate this assumption we performed numerical simulations of single axisymmetric cells for three configurations subjected to various loading paths [1]. We considered three cases: a) a cylindrical matrix containing a spherical void, b) a void-containing spherical lead inclusion, and c) a spherical lead inclusion. These configurations were subjected to compression, tension and torsion-like loading to investigate a wide range of stress triaxialities. The calculations show that in most of the loading cases (the exception being, of course, under pure hydrostatic pressure) the presence of a voided lead inclusion does not significantly affect the mechanical response of the cell; in some loading cases even the presence of a solid lead inclusion does not change the response of the single cell. Thus, in this paper, we indiscriminately assimilate void containing lead inclusions, and lead inclusions to voids.

3. Experimental procedure

3.1. Tested material

For this investigation, we are using a leaded brass, alloy 90A from Swissmetal. We fabricated all the specimens from 40 mm diameter round bars. Table 1 provides the chemical composition of the material, whereas Table 2 lists the mechanical properties provided by Swissmetal and those determined from our own tensile tests.

Table 1 - Chemical composition of Swissmetal alloy 90A (in % by weight)

Cu	Ni	Zn	Sn	Pb	Other elements
88.0-90.0	≤ 0.4	Rem.	≤ 0.1	1.5-2.2	Fe ≤ 0.1

Table 2 - Tensile properties of Swissmetal alloy 90A

	E [GPa]	Rp0.2 [MPa]		Rm [MPa]		A5 [%]	
		Min	Max	Min	Max	Min	Max
Swissmetal	119	100	360	270	410	35	10
Experiment	126	273		302		20	

3.2. Specimen geometry and test procedure

We fabricated thin-walled tubular specimens, as illustrated in Figure 1, with an N5 surface finish. We tested these specimens in pure torsion tests (PT) with no axial load, in tension-torsion tests (TT1) with an axial load of 10’180 N (90 MPa

applied nominal stress) and in tensile-torsion tests (TT2) with an axial load of 20’360 N (180 MPa applied nominal stress).

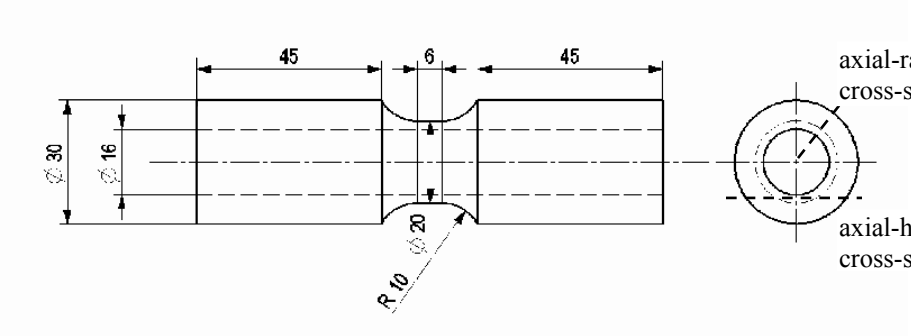

Figure 1 – Thin walled tubular specimen for torsion and combined tension-torsion tests

We performed the tests using a 100 kN / 1100 Nm tension-torsion MTS servo-hydraulic testing machine. The axial force, axial displacement, rotation angle and torque were measured using built-in transducers and load cells. For the TT1 and TT2 tests, the specimens were first preloaded in axial direction to the desired axial load at a displacement rate of 0.0167 mm/s and then the load was maintained constant during torsional loading at a rotation rate of 0.18 deg/sec. For each loading configuration, we tested three samples until fracture. In the case of the PT experiments, because of the limited angle of rotation of the hydraulic machine, we had to unload the specimens after reaching the maximal rotational stroke and reset the actuator back to its initial position. We then reloaded the specimens according to the procedure described above. The experimental records indicated no reverse plasticity upon unloading. For each loading configuration, we averaged the results of the three performed tests to obtain one representative mean loading curve.

3.3. Quantitative metallography

We performed quantitative metallography on both undeformed and tested samples. For each loading condition, we analyzed one of the three tested samples to quantify void growth and establish coalescence mechanisms. Selected samples containing an arrested crack were cross-sectioned (axial – hoop and axial – radial cross-sections, see Figure 1 and Figure 2) for metallographic preparation. We took SEM pictures below the fracture surface in randomly selected zones of equal loading and deformation, using back scattered electron (BSE) imaging to highlight the presence of lead, which decorates every void (Figure 2).

We analyzed the SEM micrographs with automated image analysis software to quantify void growth. We assumed that the observed voids have the shape of an ellipsoid that can be characterized by its three principal axes. Major axis, first minor axis and inclusion area are measured in axial – hoop cross-sections. The second minor axis is measured in axial – radial cross - sections. In performing the

image analysis, we considered the Feret diameter of the inclusion as the equivalent ellipsoid major axis. The equivalent first ellipsoid minor axis is then calculated assuming that the areas of the equivalent ellipse and of the actual inclusion are the same. Finally, the Feret diameter obtained from the axial – radial cross section provides the equivalent ellipsoid second minor axis. Results were verified independently by manual measurements of selected inclusions. We normalized all the measured cumulative size distributions of inclusions with respect to a surface of 1 mm^2.

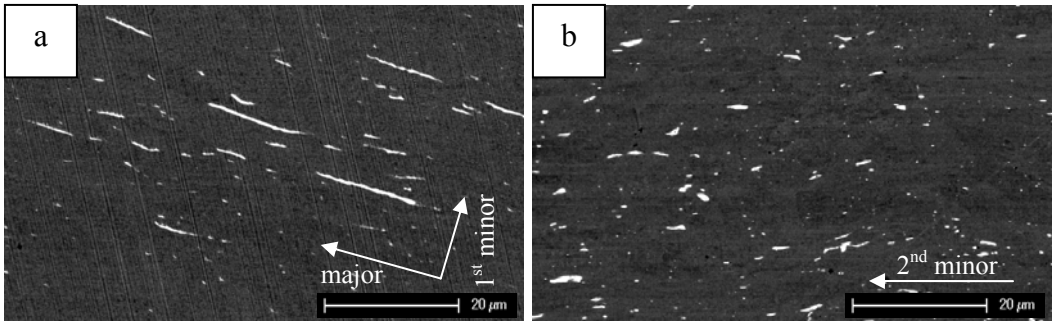

Figure 2 – BSE – SEM micrographs of polished PT specimens, a) axial – hoop cross-section, and b) axial – radial cross-section.

4. Experimental results

4.1. Macroscopic behavior

Figure 3 presents macroscopic results of PT, TT1 and TT2 experiments. Continuous lines represent mean curves of stresses or axial displacements as a function of the rotation angle. The crosses at the end of the mean curves represent actual failure points of tested samples. We notice that increasing axial load not only decreases the maximum torque and twist angle supported by the specimen, but also increases the axial displacement of the gripping ends. Somewhat surprisingly, we also note a non-negligible axial elongation in the PT specimens of 0.44 mm (average value for 3 tests)[‡].

This axial elongation is associated with a slight necking of the specimen gage section inducing a reduction in diameter of approximately 0.5 mm at the specimen symmetry plane, while the wall thickness of the tube remains essentially unchanged.

A volume estimate of the deformed PT specimen gage based on the measured dimensional changes suggests a volume increase of approximately 5%, compared to the undeformed configuration.

[‡] A similar elongation was already reported in PT tests on a high strength steel [2]-[4].

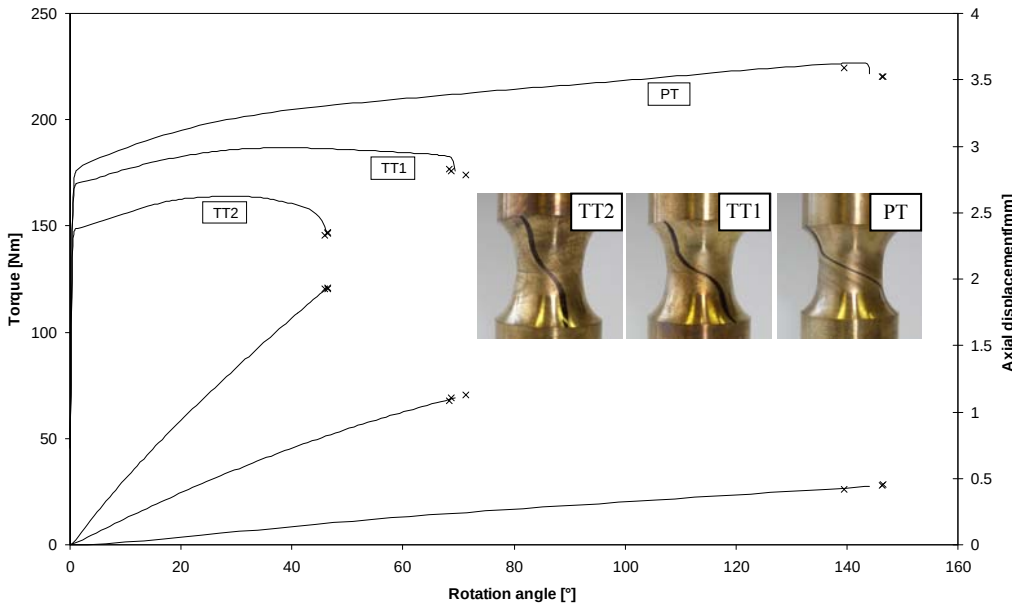

Figure 3 – Torque and axial displacement versus twist angle for torsion and tension-torsion experiments.

4.2. Evolution of void size, shape and orientation

Figure 4 illustrates the evolution of the main inclusion parameters defined in paragraph 3.3 assuming inclusions of ellipsoidal shape, namely, major axis, area, first and second minor axes (this latter parameter only for the PT specimens). In the figures, we plot the cumulative number of inclusions with a characteristic parameter greater than a certain value. We compare the distributions for the undeformed material (UD) with those for the PT, TT1 and TT2 specimens loaded to fracture.

The geometric data in Figure 4a, b and d indicate that the initial void shape is already ellipsoidal with the major axis oriented in the axial direction of the specimen. These shape and orientation result from the manufacturing process of the round bars that were used for machining our samples. For all loading conditions, we observe in Figure 4a a large increase of the major axis compared to the UD material; this elongation is associated with a significant rotation of the major axis with respect to the main specimen axis, as visible in Figure 2a. As we can expect, the increases in major axis and its rotation correlates with the specimen twist angle at fracture (see Figure 3).

Figure 4c presents the distribution of the first minor axis of the inclusions for the UD and deformed material. We observe that for each loading history, the minor axis of the deformed voids has decreased slightly compared to the UD material. This axis has also undergone a rotation coupled with the rotation of the major void axis (Figure 2a). Figure 4d presents some preliminary measurements of the

length distribution of the second minor axis for UD material and material from the PT specimens. We observe that the second minor axis also elongates significantly.

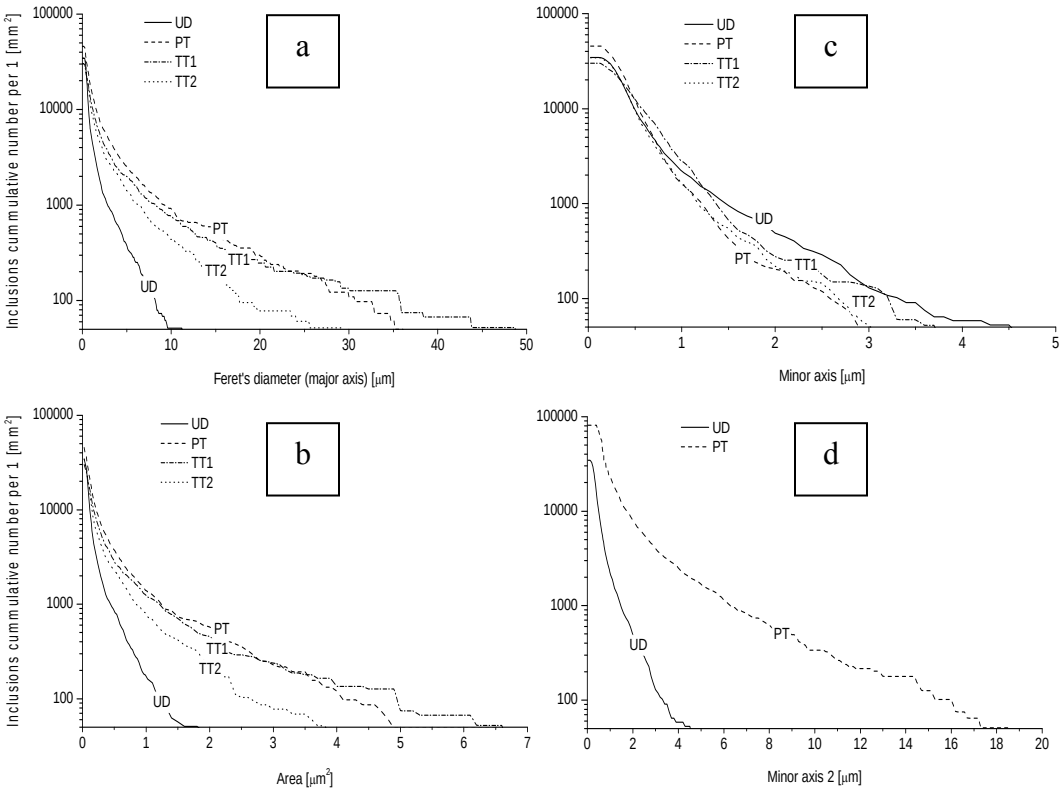

Figure 4 – Void kinetics data (equivalent ellipsoid assumption) a) major axis, b) area in axial-hoop plane, c) first minor axis and d) second minor axis.

Assuming that the initial voids are all geometrically similar and that the relative elongation of the ellipsoid axes is independent of the absolute void size, (the second assumption roughly supported by our experimental observations), we can estimate the volume change associated with the observed void growth in the PT specimens. We find that the void volume fraction in the PT specimens should be on the order of 8% compared to 1.4 % in the UD specimens. This rough estimate is somewhat higher then the estimate of the specimen volume change from macroscopic measurements, but is not inconsistent.

4.3. Micromechanisms of fracture

The void size distribution plots of Figure 4 provide a wealth of quantitative information for development and validation of void growth models. To obtain information on void coalescence processes, we need to analyze fracture surfaces of failed specimens and cross-sections of failed specimens and specimens from interrupted tests. Such analyses are ongoing and in the present paper we restrict ourselves to fracture surface observations.

Figure 5 presents fracture surfaces of PT (a, b), TT1 (c, d) and TT2 (e, f) specimens. Micrographs on the left (a, c, e) are secondary electron (SE) views, appropriate for observing the topology of the voids, and pictures on the right are corresponding micrographs of the same areas, taken by back scattered electron (BSE) imaging to highlight chemical composition, specifically lead-rich regions, appearing with a light contrast. All micrographs were taken at the same magnification for easier comparison.

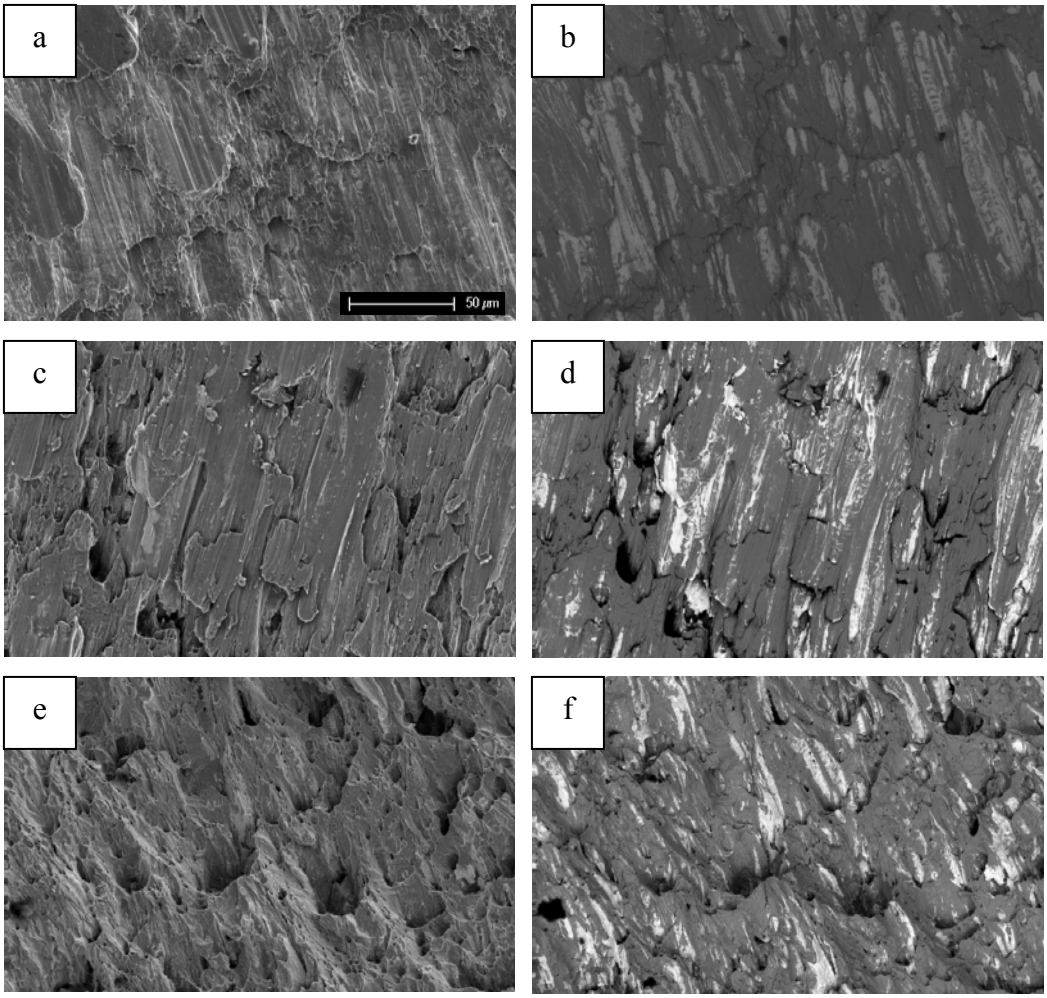

Figure 5 – SEM pictures of fracture surfaces a,b) PT, c,d) TT1, e,f) TT2 fracture surfaces

Although the fracture surface appearance varies with loading condition (compare Figure 5a and c), Figure 5 suggests that the same mechanism of void coalescence dominates final fracture in all specimens: necking of the intervoid ligament, a classical mechanism. Necks form between large voids that accelerate the growth of smaller voids in the ligament. In turn, necks form and fail between the smaller

voids, contributing to the general failure of the large necks and the lace appearance of their edges.

The difference in appearance of the specimens in Figure 5a, c and e arises 1) from the difference in orientation of the principal stress axis with respect to the void major axis (resulting from the different level of axial loading and from the material rotation), 2) from the different deformed shape of the voids and 3) possibly from localized rubbing of the fracture surfaces against each other. Observations of cross-sections indicate that the coalescence mechanisms take place in an annular region of the specimen having an axial thickness of 30 to 100 μm in PT loading up to 300 μm in TT2 loading.

5. Discussion and conclusions

In this paper, we present very early results of an experimental study of ductile void growth and coalescence under a range of stress states. We still need to analyze these results in more detail (e.g. numerical simulations to obtain stress and deformation states, improved statistics on void size distributions, interrupted tests), and to augment them with additional tests on notched tensile bars. Nevertheless, they already allow us to make several stimulating observations for further research and to draw a few preliminary conclusions.

First, we validated the approach of using a lead doped brass to get quantitative void growth data. Although we need to refine the measurement techniques and perform additional checks of the statistical relevance of the results, Figure 2 and Figure 4 exemplify the quality of the information that can be obtained. Measurements of void growth similar to those reported in Figure 4 were already reported in the literature (i.e. [5]). The novelty of our results is that we have obtained data for very large strains and material rotations, as well as under various stress states, particularly low stress triaxialities.

Second, in PT experiments we observe an elongation of the specimen in the direction of the twist axis. We already observed such an elongation in similar experiments on a high strength steel [2]-[4], in which fracture is controlled by void nucleation and not growth and coalescence. The effect of the lengthening of a tubular specimen along the principal axis about which it is being twisted is known as the Poynting or the Swift effect. Poynting [6]&[7] analyzed the behavior of isotropic materials. He attributed the origin of lengthening to the difference between axial components of the stress between internal and external ligaments. In order to equilibrate the stress components the wire as a whole must lengthen. The effect observed by Poynting in elastic wires was also observed by Swift [8] in tubular specimens in the plastic deformation regime. The permanent lengthening of a tubular specimen was also reported by Billington [9] in aluminum, copper and iron, or Miller and McDowell [10]-[11] in 304L stainless steel. More recently Weber et al. [12] observed the opposite effect of shortening in highly anisotropic alumina fiber reinforced aluminium wires. The changes in

length are attributed to anisotropy [13], e.g. due to preferential orientation of grains, or more recently to the evolution of crystallographic texture within the material [14]-[18]. At this stage, we have only conjectures regarding the mechanism of this elongation: we suspect that three dimensional constraint effects on the specimen gage length by the specimen gripping sections play a significant role for the very high twist angles involved. Although none of the mentioned authors reported increase of volume, in PT tests we also have indications of a significant increase in void volume fraction which correlates roughly with the increase in total volume of the specimen gage length.

Third, the shape of the measured void size distributions indicate that the relative growth of voids is size independent, as postulated in most models.

We are pursuing the investigation by performing interrupted PT, TT1 and TT2 tests to quantify void growth as a function of deformation (load) level. The interrupted tests will also provide details of the coalescence process. The range of stress states will be widened by testing notched tensile bars and applying the method outlined in this paper to the tested specimens.

Overall the type of data presented in this paper should prove helpful in developing, calibrating and validating more reliable and generally valid void growth and coalescence models.

6. Acknowledgements

This investigation was supported by the Swiss National Science Foundation (Project FNS 200020-107473). The authors thank Dr Claudio Penna and Dr Natanael Dewobroto from the Swissmetal for their support.

7. Literature

[1] T. Jodlowski, J.H. Giovanola, and D. Cannizzaro, On the use of model materials to investigate and quantify ductile fracture processes, *in preparation*

[2] D. Cannizzaro, Mechanisms of void initiation at small hard particles and implications for ductile fracture, Thèse sciences, EPF Lausanne, no 3579 (2006)

[3] D. Cannizzaro, J. Giovanola, R. Doglione, and A. Rossoll, Observations of ductile fracture processes under very low triaxiality in VAR steel and preliminary interpretation, Proceedings of the 11th International Fracture Conference, IFC 11, Torino, March 2005

[4] J. Giovanola, D. Cannizzaro, R. Doglione., and A. Rossoll, Ductile fracture by void nucleation at carbides, Fracture of Nano and Engineering Materials and Structures, Gdoutos, E.E. Ed Proceedings of the 16 European Conference on Fracture, Alexandroupolis, Greece, July 3-7, 2006

[5] D.R. Curran, L. Seaman, D.A. Shockey, Dynamic failure of solids, Physics Reports 147 (5-6) (1987) 253-388
[6] J.H. Poynting, On pressure perpendicular to the shear-planes in finite pure shears, and on lengthening of loaded wires when twisted, Proceedings Roy. Soc. London A 82 (1909) 549–556
[7] J.H. Poynting, On the changes in the dimensions of a steel wire when twisted, and on the pressure of distortional waves in steel, Proceedings Roy. Soc. London A 82 (1912) 534–561
[8] H. Swift, 1947. Length changes in metals under torsional overstrain, Engineering 163 (1947) 253–257.
[9] E.W. Billington, Non-linear mechanical response of various metals: II. Permanent length changes in twisted tubes, J. Phys. D: Appl. Phys. 9 (1976) 533-552
[10] M.P. Miller, D.L. McDowell, Modeling large strain multiaxial effects in FCC polycrystals, International Journal of Plasticity 12 (7) (1996) 875-902
[11] M.P. Miller, D.L. McDowell, The effect of stress-state on the large strain inelastic deformation behavior of 304L stainless steel, Transactions of the ASME 118 (1996) 28-36
[12] L. Weber, B. Moser, H.U. Kunzi, A. Mortensen, Swift and inverse swift effect in alumina fiber reinforced aluminium wires, Acta Materialia 48 (2000) 2451-2459
[13] R. Hill. The mathematical theory of plasticity, Oxford University Press, 1998
[14] F. Montheillet, M. Cohen, J.J. Jonas, Axial stresses and texture development during the torsion testing of Al, Cu, and α-iron, Acta Metallurgica 32 (11) (1984) 2077–2089
[15] F. Montheillet, P. Gilormini, J.J. Jonas, Relation between axial stresses and texture development during torsion testing: A simplified theory. Acta Metallurgica 33 (4) (1985) 705–707
[16] L.S. Tóth, J.J. Jonas, P. Gilormini, B. Bacroix, Length changes during free end torsion: A rate sensitive analysis, International Journal of Plasticity 6 (1) (1990) 83-108
[17] L.S. Tóth, P. Gilormini, J.J. Jonas, Effect of rate sensitivity on the stability of torsion textures, Acta Metallurgica 36 (12) (1988) 3077-3091
[18] A. Rohatgi, J.J. Jonas, S. Shrivastava, Effect of stress-relief annealing on the inverse Swift effect in steel and iron, Scripta metallurgica et materialia 32 (5) (1995) 737-741